Grand Potential, Helmholtz Free Energy, and Entropy Calculation in Heterogeneous Cylindrical Pores by the Grand Canonical Monte Carlo Simulation Method

Joël Puibasset

Grand potential, Helmholtz free energy and entropy calculation in heterogeneous cylindrical pores by the Grand Canonical Monte Carlo simulation method

*Joël Puibasset**

Centre de Recherche sur la Matière Divisée, CNRS-Université d'Orléans, 1b, rue de la Ferollerie, 45071 Orléans cedex 02, France

puibasset@cnrs-orleans.fr

RECEIVED DATE

ABSTRACT (Word Style "BD_Abstract"). The adsorption of fluids in porous media is still an open area of research, since no model is able to explain all experimental features. The difficulties rise from the complexity of the real porous materials which present surface heterogeneities, large pore size distributions, and complex networks of interconnected pores. In parallel to experimental efforts trying to produce more ordered porous materials, theoreticians try to introduce more disorder in their models, with the help of molecular simulation for instance. This Grand Canonical Monte Carlo simulation study concentrates on the adsorption of a simple Lennard-Jones fluid in three porous substrates, in order to compare the effect of purely geometric heterogeneity (spatial deformation of the external potential) as

opposed to purely chemical heterogeneity (amplitude variations of the external potential). This separation is unrealistic, since geometric fluctuations of a real pore diameter along its axis generally induce variations in the amplitude of the external potential created by the pore. However it enables to compare both effects. In this paper, a thermodynamic integration scheme is applied to a complete set of adsorption / desorption isotherms. The grand potential, free energy and entropy are calculated, which allows to discuss the features of the phase diagrams. It is shown that a purely geometric deformation (undulation) of the external potential does not affect the thermodynamic characteristics of the confined fluid. On the other hand, amplitude modulation of the external potential (chemical heterogeneity) strongly distorts the phase diagram. This heterogeneity is actually able to stabilize a “bridge-like” phase which corresponds to an accumulation of molecules in the most attractive region of the pore.

KEYWORDS (Word Style “BG_Keywords”). Lennard-Jones, Adsorption, Desorption, Isotherm, Hysteresis, Confinement, Disorder, Heterogeneity, Constrictions, Monte Carlo, Free Energy.

INTRODUCTION

Considerable efforts have been devoted to study the behavior of confined fluids[1-10], specially in disordered porous materials.[11-21] The introduction of heterogeneities (which is a first step before considering realistic disorder) is still a challenge due to complexity in calculations. However, molecular simulation techniques[22-24] allow to calculate the dynamical, structural and thermodynamic properties of a fluid confined in realistic porous materials, which can be compared to experiments. The Grand Canonical Monte Carlo method consists in sampling the Grand Canonical statistical ensemble, where the volume, the temperature and the chemical potential are kept constant. The acquisition of the adsorption and desorption isotherms (*i.e.* the amount of particles adsorbed in the porous material as a function of chemical potential) and the total energy of the system enables to calculate the grand potential for all thermodynamic states.[13, 14, 25-28] This characterizes completely the system and allows to determine all thermodynamic quantities as the Helmholtz free energy, or the entropy.

The heterogeneity of a realistic pore is a combination of geometric and chemical variations. To separate both effects, three pores are considered : firstly, a perfectly cylindrical pore, as a reference. Secondly, a geometrically undulated pore deduced from the previous one by simple spatial deformation of the external potential, and finally a chemically heterogeneous cylindrical pore obtained by a modulation of the depth of the external potential. This artificial separation between geometric and chemical heterogeneity is intended to enlighten their respective effects.

THE POROUS SYSTEMS

The porous models essentially derive from an atomistic description of a perfectly cylindrical pore. All interactions are modeled according to the simple Lennard-Jones (6,12) potential

$$u_{ij}(r_{ij})=4\varepsilon_{ij}[(\sigma_{ij}/r_{ij})^{12}-(\sigma_{ij}/r_{ij})^{6}] \quad (1)$$

The parameters used to describe the fluid-fluid and fluid-wall interactions are given in Table 1. They correspond to argon adsorbed in a porous solid carbon dioxide matrix. With this particular choice, the fluid has strong affinity with the wall, compared to fluid-fluid interaction, which enhances the surface effects in confinement situations. This system has already been chosen to study phase diagrams of fluids confined in cylindrical pores[7-9, 19, 29], but it is now extended to heterogeneous porous substrates. Comparisons are then possible. In the following, all quantities are normalized to the argon-argon parameters. For instance distances and energies are given in units of σ_{f-f} and ε_{f-f}.

The pores considered are nanometric, 2.724 nm in diameter, which corresponds exactly to 8 atomic diameters (σ_{f-f}). This way, the smooth-wall approximation can be applied: the external potential seen by a fluid particle in the pore is calculated by integrating the Lennard-Jones potential over a uniform distribution of wall interacting sites. The substrate site reduced density is taken equal to $\rho^{*}_{solid}=\rho_{solid}\sigma_{f-f}^{3}=0.8265$ which corresponds to solid CO_2 of density 1530 kg/m^3. The calculated external potential ψ_{cyl} in this perfectly cylindrical pore has a cylindrical symmetry, and can be given as a function of the radial distance only. The reduced potential $\psi^{*}_{cyl}(r)=\psi_{cyl}(r)/\varepsilon_{f-f}$ is shown in Figure 1

The heterogeneity is introduced by modulating the external potential. In the first case, geometric heterogeneity is produced by spatially deforming the potential, while in the second case, chemical heterogeneity is created by modulating the amplitude of the initial cylindrical potential. In both cases the

modulation along the axial direction *z* introduces an explicit dependence of the potential on *r* and *z*. The geometrically heterogeneous reduced potential is given by:

$$\psi^*_{geo}(r,z)=\psi^*_{cyl}\left(r/\left\{1-a\cos\left(\frac{2\pi z}{L}\right)\right\}\right) \quad (2)$$

and the chemically heterogeneous reduced potential is given by:

$$\psi^*_{chem}(r,z)=\left\{1+a\cos\left(\frac{2\pi z}{L}\right)\right\}\psi^*_{cyl}(r) \quad (3)$$

The parameter *a* is a measure of the amplitude of the heterogeneity, taken equal to 0.25 in this work, and L is the length of the simulation box, equal to $12\sigma_{f-f}$ in the direction of the z coordinate. The contour plots of the external potentials are given in Figure 2, in the plane defined by the radial and axial coordinates. As can be seen the external potential in the perfectly cylindrical pore is invariant along the axial coordinate, which is not the case for both undulated pores. The contour lines correspond to increments of 0.05 in reduced potential, and correspond to the horizontal lines in Figure 1 for the cylindrical pore. The radius of the geometrically undulated pore varies between $3\sigma_{f-f}$ for $z=0$ and $5\sigma_{f-f}$ for $z=\pm L/2$. In this system, the heterogeneity consists in an enlargement of the pore size distribution up to 25% of its average value. For the second system the pore radius is constant, but the intensity of the fluid-wall interaction varies within 25% of its average value: this mimics some chemical heterogeneity with more or less attractive sites distributed along the pore. It is important to note that the geometric modulation has not been applied to the solid CO_2 prior to the potential calculation. This would have been certainly more realistic, but it would have induced the appearance of zones of higher potential in the regions of higher curvature for instance. In this work we wanted precisely to decouple geometric from amplitude modulation effects.

To enlighten the energetic characteristics of the pore, one can evaluate the volume distribution of the external potential, that is to say the density of volume of the pore which is at a given external potential. Let us consider the volume dV^{Ψ} of all the regions of a given pore of total volume V where the external

potential is between Ψ and Ψ+dΨ. Let us define the volume fraction density ν of the pore at a given potential Ψ as:

$$\nu(\Psi) = \frac{1}{V}\frac{dV^{\Psi}}{d\Psi} \tag{4}$$

This quantity is drawn in Figure 3. As can be seen, the volume distribution of the external potential in the perfectly cylindrical pore has two peaks. The large one close to zero corresponds to the region of the pore in the vicinity of the axis, whereas the smaller peak close to the minimum of Ψ=-3.8 corresponds to the regions of the pore in the vicinity of the substrate wall. For Ψ above zero, the distribution is very close to zero since the potential varies very rapidly. The total integral of the distribution, up to infinity, is equal to 1. The volume distribution of the geometrically undulated pore is exactly the same as the one for the perfectly cylindrical pore due to the simple geometric deformation. This means that, regardless of the spatial distribution of the potential, the energetic characteristics of the pores are identical. They only differ from a topological point of view. This justifies the construction of this pore by geometric deformation of the initially cylindrical potential, instead of recalculating the real potential in an undulated pore: changing the topology without changing the energetic characteristics of the pore. On the other hand, the volume distribution of the external potential in the chemically heterogeneous pore is significantly affected, showing a spreading of the low Ψ peak to much lower values of Ψ. The small and diffuse peak around -2.8 is from the contribution of the pore in the vicinity of the substrate wall in the region around z* = ±6.

Another way to characterize the energetic properties of a pore is to calculate the space integral of the exponential of minus the external potential ψ^*_{ext} over the accessible reduced volume V^*, which, by definition, is the volume of space where the potential is not infinite:

$$A(T^*) = \frac{1}{V^*}\int e^{-\Psi^*_{ext}/T^*} d\mathbf{r}^* = \int \nu(\Psi^*_{ext}) e^{-\Psi^*_{ext}/T^*} d\Psi \tag{5}$$

The numeric results for $A(T^*)$ for the cylindrical, the geometrically and the chemically modulated pores are given in Table 2. As can be seen, the space integral in the geometrically undulated pore is exactly the

same as in the perfectly cylindrical one. On the other hand, the space integral $A(T^*)$ is larger for the chemically modulated pore, because this modulation creates zones of lower potential (see Figure 3) which contribute the most to the integral.

ADSORPTION / DESORPTION ISOTHERMS AND CONFIGURATIONAL ENERGY

The system consists in argon particles confined in the three external potentials ψ^*_{cyl} , ψ^*_{geo} , ψ^*_{chem} . The size of the simulation box in the axial direction is equal to $12\sigma_{f-f}$. The extension in the radial direction is limited by the external potential. The fluid-fluid interactions are calculated without distance cut-off, and with minimal image convention. The Grand Canonical Monte Carlo simulation (GCMC) consists in generating a series of molecular configurations according to the Grand Canonical statistical ensemble, where the system can exchange particles and energy with a reservoir which imposes constant temperature and chemical potential. Therefore, it mimics a real adsorption experiment where volume and temperature are controlled and the chemical potential is fixed through the pressure of the gas reservoir. From a technical point of view, the simulation consists, on the one hand, in thermal equilibration of the simulation box through molecular displacements with acceptance probabilities determined by the ratio of the difference in energy to the external temperature, and on the other hand, in chemical equilibration with a particle reservoir through addition or removal of particles in the simulation box with probabilities determined by the imposed chemical potential. For a complete and detailed explanation of the technique, see ref [22-24]. During the course of the simulation, the total number N of particles in the box and the total reduced configurational energy U* are averaged. Two reduced quantities are then generated for each reduced temperature T^* and reduced chemical potential μ^* considered as parameters: the reduced average coverage Γ^*=N/V* where V* is the reduced accessible volume, and the reduced average configurational energy per particle u^*=U*/N. By definition, the accessible volume is the volume of space where the potential is not infinite. This definition is identical

to the one used by other authors in previous publications.[7-9, 19, 29] For instance, in the case of the perfectly cylindrical pore of length L, the external potential is infinite for a reduced radial distance of 4. As a consequence, the accessible volume is $V_{cyl}=16\pi L\sigma_{f-f}^{2}$. The accessible volume of the chemically heterogeneous pore is exactly the same since both potentials are infinite in the same region of space: $V_{chem}=16\pi L\sigma_{f-f}^{2}$. The accessible volume of the geometrically undulated pore is calculated by integration of the sinusoidal modulation: $V_{geo}=16.5\pi L\sigma_{f-f}^{2}$. It is slightly larger than the cylindrical volume.

In a real adsorption experiment, the adsorbate is introduced progressively to get adsorbed in the previously out-gassed porous sample. Similarly, the initial molecular configuration is the empty pore, used as the starting point of the simulation at very low chemical potential. The chemical potential of the gas reservoir is then increased step by step to calculate the whole adsorption isotherm. For each step, the initial configuration is the final configuration of the preceding step. At least 10^5 Monte-Carlo trials per molecule are performed to reach equilibrium, and then at least twice as many to acquire statistics. When the saturation of the sample is reached, one can start to calculate the reverse path by decreasing the pressure. The obtained so-called desorption branch is generally not identical to the adsorption branch (hysteresis).

The adsorption and desorption isotherms have been calculated in the three pores at six reduced temperatures: 0.60, 0.77, 0.82, 0.90, 1.00 and 1.20. The results for Γ* (reduced coverage) are shown as a function of the chemical potential in the Figure 4 for the perfectly cylindrical pore, the geometrically and the chemically undulated pores. The average coverage Γ* is drawn on a semi-logarithmic scale to enhance the low coverage region. The straight lines represent the ideal gas approximation adsorption isotherms:

$$\Gamma^*_{id}=\frac{e^{\mu^*/T^*}}{\Lambda^{*3}}\left[\frac{1}{V^*}\int d\mathbf{r}^* e^{-\Psi^*_{ext}/T^*}\right] \qquad (6)$$

obtained by integrating the "barometric law"[30], where Γ^*_{id} is the reduced coverage for the ideal gas, μ^* the reduced chemical potential, Λ^* the reduced de Broglie's wave length, and the integral of the exponential of the external potential ψ^*_{ext} is performed over the accessible reduced volume V^*. The space integral between brackets was previously introduced in Equation 5. Its numerical value, as well as de Broglie's wavelengths, are given at different temperatures for the three pores in Table 2. Since the space integral between brackets is identical for the perfectly cylindrical and the geometrically deformed pores, their ideal gas approximation adsorption isotherms are identical. On the other hand, the ideal gas adsorption is larger in the chemically heterogeneous pore. All adsorption isotherms calculated for the interacting gas converge to the ideal gas limit at low coverage, where fluid-fluid interactions are negligible. The higher the temperature the larger the amount adsorbed for a given chemical potential. However, for large chemical potential the coverage in the porous substrate saturates independently of the temperature due to hard core repulsion in the fluid. The low temperature curves show jumps and large hysteresis in the amount adsorbed. For instance, in the perfectly cylindrical pore, at T*=0.60, the amount adsorbed follows the ideal gas approximation up to μ^*=-9.6, then increases faster up to μ^*=-9.0 and Γ^*=0.034 where it abruptly jumps to Γ^*=0.64. The chemical potential was increased by small increments in this region of jump, which allows to show an almost vertical line. It is important to note that despite the presence of vertical lines (guides to the eyes), it was actually impossible to stabilize the reduced coverage to any intermediate value between Γ^*=0.034 and Γ^*=0.64 (absence of simulation points on the Figure 4 along the vertical lines). If the chemical potential is now decreased, one follows the T*=0.60 desorption (liquid-like) branch, down to μ^*=-10.36, that is to say one does not follow the previous adsorption isotherm: the adsorption / desorption phenomenon is not reversible at such a low temperature and presents an hysteresis. However, as can be seen, the higher the temperature, the narrower the hysteresis loop (see Figure 4), in agreement with experimental observations[31, 32], and theoretical aclculations[4]. At T*=1.00, the hysteresis is very thin, but the vertical jump is still visible. However, at T*=1.20, the adsorption curve is perfectly reversible (supercritical adsorption isotherm). This set of adsorption isotherms looks like that of a first order liquid-gas transition. The isotherms

present a discontinuity with two clearly distinguishable metastable phases (hysteresis), like for a Van der Waals loop. Furthermore, the high temperature isotherm is reversible, which shows that the hysteresis has to vanish in a so-called hysteresis critical point T_{ch} [31, 32] between T*=1.00 and T*=1.20. However, in cylindrical pores the phase transition is necessarily rounded, but still sharp enough to be considered as a phase transition.[33] The vertical dotted segments correspond to the chemical potential value for which the grand potential is identical (equilibrium coexistence point) for the two phases indicated by the two ends of each segment (to be discussed later).

The introduction of a geometric undulation is expected to strongly affect this set of adsorption isotherms, due to confinement effects. However, inspection of Figure 4 shows only minute differences between the geometrically undulated pore and the perfectly cylindrical pore. In a realistic confinement situation, it is not only the accessible space for the confined particles which is modified, but also the depth and shape of the external potential felt by the particles. However, in our simulation study, the geometrically undulated pore is obtained by a purely geometrical deformation of the external potential, without changing the distribution of volume of space having a given value of external potential (see Figure 3). The main consequence is the invariance of the space integral defined by Equation 5. The similarity of the adsorption isotherms shows, firstly, that the topologies of both pores are close enough not to introduce differences, and, secondly, that the adsorption properties are not very sensitive to the spatial shape of the potential, but are closely related to the volume distribution of the external potential $\nu(\Psi)$ defined by Equation 4. However, there is some differences: hysteresis loop is slightly narrower in geometrically undulated pores compared to perfectly cylindrical pore. This might be due to some destabilization of the fluid due to geometric undulation (local curvature) which could help the nucleation of the low density phase.

On the other hand, the introduction of chemical heterogeneity in the pore strongly affects the adsorption isotherms, as can be seen on Figure 4. Firstly, quantitative changes can be noted: larger

amount adsorbed for a given chemical potential, lower “critical temperature” since the adsorption isotherm for T*=1.00 is now reversible, and finally thinner hysteresis loops. Secondly, the isotherms are qualitatively modified, since now three branches (or “phases”) can be observed for the lowest temperatures. For instance, if one follows the isotherm at T*=0.77, starting from low chemical potential, the average coverage jumps to an intermediate value of 0.28 for μ*=-10.60 before it jumps again to a liquid-like value of 0.55 for μ=-10.53. If one decreases now the chemical potential, the average coverage will drop abruptly directly to the gas-like value for μ=-10.72, without going through the “intermediate phase”. However, it is possible to jump from the “intermediate phase” to the gas-like phase by decreasing the chemical potential directly from μ=-10.60 without passing by the liquid-like phase. The instability point in this case is at μ =-10.62, that is to say higher than the liquid instability point (μ =-10.72), which explains why the liquid phase jumps directly to the gas phase below its instability point. As can be noted, this state of intermediate density has been qualified as a phase by analogy with both the gas-like and liquid-like phases. It might be abusive, although practical. However, such a state has already been observed by other authors, and has been called ‘bridge phase”.[28, 34-36] This phase is essentially made of the accumulation of molecules (with local density close to the liquid) in the attractive region of the pore. For coherence, the same name will be used in the rest of the paper .The T*=0.90 isotherm does not show three branches. Actually, the gas-like branch is reversible up to an average coverage corresponding to the intermediate phase. It means that the analog to the critical temperature associated to the gas-like to bridge-like transition is lower than 0.90. However, the bridge-like to liquid-like transition is still visible with a small hysteresis loop at T*=0.90.

The Figure 5 shows the reduced configurational energy per particle, u*, as a function of the chemical potential, for the three pores and the same temperatures as for the average coverage. The low density or low chemical potential limit is in good agreement with the ideal gas approximation values given in Table 3 according to the formula:

$$u^*_{id} = \frac{1}{\Gamma^*_{id}} \frac{1}{V^*} \int \Psi^*_{ext} \rho^*_{id} d\mathbf{r}^* = \frac{1}{V^* A(T^*)} \int \Psi^*_{ext} e^{-\Psi^*_{ext}/T^*} d\mathbf{r}^* \quad (6)$$

where *id* is for ideal gas, ρ^*_{id} is the local ideal gas density in the pore, V* is the total reduced volume of the pore, and *A(T*)* has been defined in Equation 5. Inspection of Figure 5 shows that the molecular configurational energy decreases as the chemical potential increases, and presents the same hysteresis as the total coverage Γ*. Comparison between the three pores shows that the differences between the perfectly cylindrical pore and the geometrically undulated pore are very small, whereas the chemical undulation introduces noticeable changes. For instance, the chemical heterogeneity stabilizes a phase of intermediate energy, and lowers the configurational energy of the gas-like phase specially in the large chemical potential region of each isotherm. One can also note that, concerning the "bridge-like" phase, contrarily to the total coverage Γ which is almost constant whatever the temperature, the configurational energy per particle significantly decreases with temperature.

GRAND POTENTIAL, HELMHOLTZ FREE ENERGY AND ENTROPY CALCULATION

grand potential calculation

From a thermodynamic point of view, a system is completely described if one is able to calculate the appropriate thermodynamic potential. More precisely, since our simulations are performed in the Grand Canonical Ensemble, the thermodynamic potential to be considered is the grand potential Ω. However, this quantity is not a direct output of the grand canonical monte carlo (GCMC) simulation. A way to circumvent this problem was proposed by Peterson and Gubbins[9]. In their method they take advantage of two differential equations to calculate the grand potential along reversible paths, from a reference point up to both the vapor and liquid branches. The two differential equations link the grand potential Ω

to the number of particles and the total energy of the system which are given by the GCMC simulation The first equation is the Gibbs adsorption isotherm, obtained by differentiating Ω along constant temperature paths:

$$\left(\frac{\partial \Omega}{\partial \mu}\right)_{T,V} = -N \tag{7}$$

where N is the number of particles in the simulation box of volume V. The second equation is obtained along paths of constant chemical potential μ:

$$\left(\frac{\partial(\Omega/T)}{\partial(1/T)}\right)_{\mu,V} = E - N\mu \tag{8}$$

where E is the total energy of the system, that is to say the sum of the configurational energy U and the kinetic energy taken equal to 3/2NkT. Let us introduce the grand potential per unit of volume $\omega = \Omega/V$, where V is the volume of the system. Since V is a constant it can be introduced in the two differential equations 7 and 8, which take the final form, in reduced units:

$$\left(\frac{\partial \omega^*}{\partial \mu^*}\right)_{T^*,V^*} = -\Gamma^* \tag{9}$$

$$\left(\frac{\partial(\omega^*/T^*)}{\partial(1/T^*)}\right)_{\mu^*,V^*} = \Gamma^*\left(u^* + \frac{3}{2}T^* - \mu^*\right) \tag{10}$$

which involve only previously introduced quantities. This set of equations allows to calculate the difference in the reduced grand potential per unit volume between any states of the system. More precisely, the integration has to be performed along a reversible path: the supercritical adsorption isotherm is then used to connect the gas-like and liquid-like phases. Additional points have been simulated in the liquid-like phase to increase the precision in the integration along constant μ paths.

To get absolute values for ω^*, one has to know at least one point. For μ low enough so that the adsorption isotherm is essentially the ideal gas approximation, one can use the ideal value for the grand potential:

$$\omega^*_{id} = -\Gamma^* T^* \quad (11)$$

This ideal gas approximation has been used for each adsorption isotherm. The result for the grand potential along all isotherms is given in Figure 6 for the three pores. As can be seen, the grand potential is multi-valued, except for supercritical temperature (reversible isotherms). In the case of the perfectly cylindrical and geometrically undulated pores, the gas-like and liquid-like branches intersect for each sub-critical temperature. These intersection points are the equilibrium points for a given temperature. They are reported on the hysteresis loops of Figure 4 as vertical dotted lines. As the temperature increases, the slopes of the grand potential along the gas-like and liquid-like branches at the intersection point tend to be identical. The two branches finally merge in a unique continuous branch at the critical temperature and above. The positions of the equilibria are very similar in the perfectly cylindrical and the geometrically undulated pores, showing again that the introduction of the purely geometric modulation does not strongly affect the thermodynamic characteristics of the pore. In Figure 6, the stable states can be determined by considering the fact that they are given by the absolute minimum of the grand potential. As a consequence, the liquid branches on the left of the intersection points and the gas branches on the right of these same intersection points correspond to metastable states of the adsorbed fluid, as for a Van der Waals fluid. On the other hand, the chemically undulated pore offers a much more interesting fluid behavior, with the existence of three branches below $T^* = 0.82$. Enlargements of the intersection regions are given in Figure 7 for the four temperatures of interest. At the lowest temperature, the new "phase" of intermediate coverage has a grand potential branch above the intersection point of the gas-like and liquid-like phases. The domain of existence of the phase is large enough to allow this branch to cross the gas-like and liquid-like branches. Then one has three intersection points, which give three possible equilibria. The most stable branches correspond to the absolute minimum of the grand potential, that is to say the gas branch for chemical potential below –9.48, and liquid branch for higher chemical potential. All other branches, in particular the "bridge phase", correspond to metastable states. The gas-bridge and the bridge-liquid equilibria are also in the metastable region. As the temperature is increased, the gas-like and the bridge-like branches move

towards lower chemical potential, relative to the liquid-like branch. It results in the existence of a temperature slightly below $T^* = 0.77$ where the three branches intersect at the same point, that is to say a chemical potential where the three "phases" can coexist (triple point T^*_{triple}). When the temperature is slightly increased up to $T^* = 0.77$, the three branches intersect again in three different points, but the gas-liquid intersection is now above the "bridge-like phase" branch. The stable states are then the gas branch for a chemical potential below $\mu = -10.609$, the bridge state for $-10.609 < \mu < -10.600$, and the liquid phase for $\mu > -10.600$. All other branches are again metastables. In particular, the gas-liquid equilibrium is now in the metastable region. As the temperature increases, the gas branch continues to shortens, and finally does not intersect the liquid branch any more for $T^* = 0.82$ (see Figure 7). The previously metastable gas-liquid equilibrium has now reached the instable region and disappears. However, the gas-bridge and bridge-liquid equilibria persist and are stable. For higher temperatures, the gas and bridge branches become more and more parallel, and finally merge in a unique branch between $T^* = 0.82$ and 0.90. The gas-bridge equilibrium then ends in a first "critical temperature" T^*_{c1} between 0.82 and 0.90. Above this temperature, only two branches are visible, which finally merge also into a unique branch between $T^* = 0.90$ and 1.00 (see Figures 6 and 7). This point defines the second "critical temperature" T^*_{c2} of the system. The phase diagram then contains at least two critical points and a triple point: such a complexity was previously observed in energetically corrugated slit pores.[21, 34-36]

Helmholtz free energy and entropy calculation

Helmholtz free energy and entropy are conceptually very important quantities which are not so commonly calculated in simulation works. This is specially the case of entropy, which is almost never calculable in a direct way, except by means of sophisticated methods (see [37] and references therein). However, in our system, since the thermodynamic state is now fully characterized through the knowledge of the reduced grand potential per unit of volume ω^*, it is possible to calculate all state functions. The reduced molecular free energy is calculated according to the formula

$$f^*=\frac{\omega^*}{\Gamma^*}+\mu^* \quad (12)$$

and plotted versus the reduced coverage Γ* in Figure 8. As can be seen, the free energy increases with coverage, and diverges for zero coverage, following the ideal gas behavior. The free energy is a continuous function of the coverage for supercritical temperature, and presents a discontinuity for subcritical temperatures. As previously, the purely geometric undulation has almost no effect on the free energy results. On the other hand, the chemical modulation introduces strong modifications of the fluid thermodynamics, with the appearance of two discontinuities at low temperatures. The gaps in the free energy surface correspond to the coexistence regions of two phases, where the free energy is given as a linear combination of the free energies of each phase. This has not been drawn for clarity.

The reduced entropy per particle is obtained from the reduced Helmholtz free energy f^* per particle and the reduced molecular configurational energy u^*, according to the formula:

$$s^*=\frac{3}{2}+\frac{u^*-f^*}{T^*} \quad (13)$$

The Figure 9 shows this quantity as a function of the chemical potential μ*. The entropy decreases with chemical potential or coverage, due to excluded volume effects. The entropy of the high density phase tends to be weakly dependent on temperature. This is again the signature of hard core repulsion. The coexistence regions are visible. The hysteresis shows again the existence of metastable states for the homogeneous phases. The coexistence phases would correspond to vertical lines at the same positions as in the Figure 4.

discussion and conclusion

This work has shown that it is possible to completely characterize the thermodynamic behavior of a confined fluid in a porous material by monte carlo simulation. It should then be possible to answer the question whether the observed transition is first order or not. In the case of the cylindrical pore, the

results show that all thermodynamic quantities present a discontinuity and an hysteresis in a certain region of parameter space. This favors a first order phase transition. Of course, it is actually impossible to affirm that the observed “jumps” in the thermodynamic quantities are real discontinuities or simply sharp variations within the small interval between two consecutive points. However, within this hypothesis of real discontinuities, the adsorption / desorption isotherms of Figure 4 would be branches of van der Waals loops. The GCMC method actually does not allow for a complete calculation of the loop, specially in the instable region. Within this scheme, the two gas-like and liquid-like branches correspond to real phases, which are obviously not homogeneous in space. This is not a drawback, as long as there is no discontinuity in the local particle density within each “phase”. Finally, it was shown that the hysteresis disappears in the cylindrical pore for a reduced hysteresis critical temperature T_{ch}^* between 1.0 and 1.2. Since T_{ch}^* is not necessarily the pore critical temperature, characterized for instance by a divergence of the compressibility, it cannot be ascertained that the critical point lies within the same interval of temperature. However, such a critical temperature should exist in the vicinity of T_{ch}.

This work has shown that the purely geometric deformation of the external potential (25% undulation) has not modified the thermodynamic properties of the confined fluid, just like it did not change the space integral defined by Equation 5, and the volume fraction density defined by Equation 4. On the other hand, a 25% modulation of the amplitude of the external potential induces strong modifications, as the depression of the initial hysteresis critical point compared to the cylindrical case, the appearance of a third branch in the adsorption / desorption curve (and a new “bridge-like” phase), a second hysteresis critical point, and a triple point temperature where the liquid-like, gas-like, and bridge-like phases are in equilibrium. These results are in agreement with theoretical and simulation results[4, 18, 28, 34-36, 38] describing the competition of ordinary liquid-gas transition with new phases stabilized by the substrate surface, like layers[18, 39] or bridge-like phases[21, 28, 34-36]

To what extent can such an analysis be applied to real porous materials? Of course, the model includes some realistic features of porous media (geometric or chemical heterogeneity). However, these heterogeneities are not as complex as the disorder characterizing realistic porous media. This is probably why the hysteresis observed in this study are “empty”, in opposition to experimental hysteresis which can be filled completely by scanning curves[1, 2]. However, the 25% chemically undulated model is able to produce a new branch within the main hysteresis loop. It is thought that the introduction of more disorder would produce a main hysteresis filled with a large number of “intermediate phases”, which would allow to draw realistic scanning curves. The author suggest that these “intermediate branches” could be connected to the numerous local minima in free energy landscape observed in density functional theory calculations on Ising-like models.[12] In such a situation, the nature of the phase transition would certainly not be first order any more, and is actually still an open question.

ACKNOWLEDGMENT. It is a pleasure to thank A. Delville, R. Pellenq, and P. Porion for very stimulating discussions throughout this work. The simulations were performed locally on workstations purchased thanks to grants from Région Centre (France).

REFERENCES

1 S. J. Gregg and K. S. W. Sing, *Adsorption, Surface Area and Porosimetry* (Academic Press, New York, 1982).

2 F. Rouquerol, J. Rouquerol, and K. S. W. Sing, *Adsorption by Powders and Porous Solids* (Academic Press, London, 1999).

3 L. D. Gelb, K. E. Gubbins, R. Radhakrishnan, et al., Reports on Progress in Physics **62**, 1573 (1999).

4 R. Evans, U. Marini Bettolo Marconi, and P. Tarazona, Journal of Chemical Physics **84**, 2376 (1986).

5 J. P. R. B. Walton and N. Quirke, Molecular Simulation **2**, 361 (1989).

[6] A. V. Neimark, P. I. Ravikovitch, and A. Vishnyakov, Physical Review E **65**, 031505 (2002).
[7] G. S. Heffelfinger, F. van Swol, and K. E. Gubbins, Molecular Simulation **61**, 1381 (1987).
[8] A. Z. Panagiotopoulos, Molecular Physics **62**, 701 (1987).
[9] B. K. Peterson and K. E. Gubbins, Molecular Physics **62**, 215 (1987).
[10] K. Bucior, A. Patrykiejew, O. Pizio, et al., Journal of Colloid and Interface Science **259**, 209 (2003).
[11] E. Pitard, M. L. Rosinberg, and G. Tarjus, Molecular Simulation **17**, 399 (1996).
[12] E. Kierlik, P. A. Monson, M. L. Rosinberg, et al., Physical Review Letters **87**, 055701 (2001).
[13] M. Alvarez, D. Levesque, and J.-J. Weis, Physical Review E **60**, 5495 (1999).
[14] R. J.-M. Pellenq and P. E. Levitz, Molecular Physics **100**, 2059 (2002).
[15] L. Sarkisov and P. A. Monson, Physical Review E **65**, 011202 (2002).
[16] J. K. Brennan and W. Dong, Physical Review E **67**, 031503 (2003).
[17] J. Puibasset and R. J.-M. Pellenq, Journal of Chemical Physics **118**, 5613 (2003).
[18] A. Vishnyakov, E. M. Piotrovskaya, and E. N. Brodskaya, Langmuir **17**, 4451 (2001).
[19] B. K. Peterson, K. E. Gubbins, G. S. Heffelfinger, et al., Journal of Chemical Physics **88**, 6487 (1988).
[20] B. Coasne and R. J.-M. Pellenq, Journal of Chemical Physics **120**, 2913 (2004).
[21] B. Millan-Malo, O. Pizio, A. Patrykiejew, et al., Journal of Physics : Condensed Matter **13**, 1361 (2001).
[22] M. P. Allen and D. J. Tildesley, *Computer simulation of liquids* (Clarendon Press, Oxford, 1987).
[23] D. Frenkel and B. Smit, *Understanding Molecular Simulation* (Academic Press, London, 1996).
[24] D. Nicholson and N. G. Parsonage, *Computer simulation and the statistical mechanics of adsorption* (Academic Press, London, 1982).
[25] K. S. Page and P. A. Monson, Physical Review E **54**, R29 (1996).
[26] K. S. Page and P. A. Monson, Physical Review E **54**, 6557 (1996).
[27] L. Sarkisov and P. A. Monson, Physical Review E **61**, 7231 (2000).
[28] J. Reszko-Zygmunt, O. Pizio, W. Rzysko, et al., Journal of Colloid and Interface Science **241**, 169 (2001).
[29] B. K. Peterson, J. P. R. B. Walton, and K. E. Gubbins, Journal of Chemical Society Faraday Transactions II **82**, 1763 (1986).
[30] J. S. Rowlinson and B. Widom, *Molecular Theory of Capillarity* (Clarendon Press, Oxford, 1982).
[31] K. Morishige and M. Shikimi, Journal of Chemical Physics **108**, 7821 (1998).
[32] K. Morishige and N. Tateishi, Journal of Chemical Physics **119**, 2301 (2003).
[33] R. Evans, Journal of Physics : Condensed Matter **2**, 8989 (1990).
[34] P. Röcken and P. Tarazona, Journal of Chemical Physics **105**, 2034 (1996).
[35] P. Röcken, A. Somoza, P. Tarazona, et al., Journal of Chemical Physics **108**, 8689 (1998).
[36] H. Bock and M. Schoen, Physical Review E **59**, 4122 (1999).
[37] S. Prestipino and P. V. Giaquinta, Journal of Statistical Physics **96**, 135 (1999).
[38] H. Nakanishi and M. E. Fisher, Journal of Chemical Physics **78**, 3279 (1983).
[39] I. Brovchenko, A. Geiger, and A. Oleinikova, Journal of Chemical Physics **120**, 1958 (2004).

FIGURE CAPTIONS (Word Style “VA_Figure_Caption”).

FIGURE 1:

Reduced external potential in the perfectly cylindrical pore as a function of the reduced radial distance.

FIGURE 2:

Contour plots of the external potentials in the three pores, in the axial and radial coordinates plane. The increment of reduced potential between contours is 0.05.

FIGURE 3:

Volume fraction density $\nu(\Psi)=\frac{1}{V}\frac{dV^{\Psi}}{d\Psi}$ of the three pores (see Equation 4) .

FIGURE 4:

Adsorption / desorption isotherms for a Lennard-Jones fluid at several temperatures, in the perfectly cylindrical pore, the geometrically and the chemically undulated pores. The vertical dotted segments materialize the coexistence points (intersection points of the grand potential of Figure 6).

FIGURE 5:

Configurational energy for a Lennard-Jones fluid at several temperatures, in the perfectly cylindrical pore, the geometrically and the chemically undulated pores.

FIGURE 6:

Grand potential for a Lennard-Jones fluid at several temperatures, in the perfectly cylindrical pore, the geometrically and the chemically undulated pores, versus the reduced chemical potential.

FIGURE 7:

Grand potential of the “bridge-phase” for a Lennard-Jones fluid at several temperatures, in the chemically undulated pore, versus the reduced chemical potential.

FIGURE 8:

Helmholtz free energy per particle for a Lennard-Jones fluid at several temperatures, in the perfectly cylindrical pore, the geometrically and the chemically undulated pores, versus the reduced coverage.

FIGURE 9:

Reduced entropy per particle for a Lennard-Jones fluid at several temperatures, in the perfectly cylindrical pore, the geometrically and the chemically undulated pores, versus the reduced chemical potential.

TABLES.

TABLE 1: Argon/solid CO_2 interaction parameters

	ε/k_B (K)	σ (Å)
fluid-fluid (f-f)	119.8	3.405
wall-fluid (w-f)	153.0	3.725

TABLE 2: De Broglie's reduced wavelength for Argon and normalized space integral $A(T^*)=\frac{1}{V^*}\int d\mathbf{r}^* e^{-\Psi^*_{ext}/T^*}$ for the perfectly cylindrical, the geometrically and the chemically undulated pores for different temperatures.

T*	De Broglie's reduced wavelength for Argon	$A(T^*)$ for the perfectly cylindrical pore	$A(T^*)$ for the geometrically undulated pore	$A(T^*)$ for the chemically undulated pore
0.60	0.0953	49.5	49.5	77.5
0.77	0.0841	14. 9	14.9	19.3
0.82	0.0815	11.6	11.6	14.5
0.90	0.0778	8.35	8.35	10.0
1.00	0.0738	6.02	6.02	6.91
1.20	0.0674	3.77	3.77	4.11

TABLE 3: Low coverage limit for the ideal gas reduced molecular configurational energy calculated in the perfectly cylindrical, the geometrically and the chemically undulated pores for different temperatures (see Equation 6).

T*	u^*_{id} for the perfectly cylindrical pore	u^*_{id} for the geometrically undulated pore	u^*_{id} for the chemically undulated pore
0.60	-3.355	-3.355	-3.923
0.77	-3.155	-3.155	-3.616
0.82	-3.096	-3.096	-3.528
0.90	-3.004	-3.004	-3.394
1.00	-2.895	-2.895	-3.238
1.20	-2.702	-2.702	-2.970

Figure 1

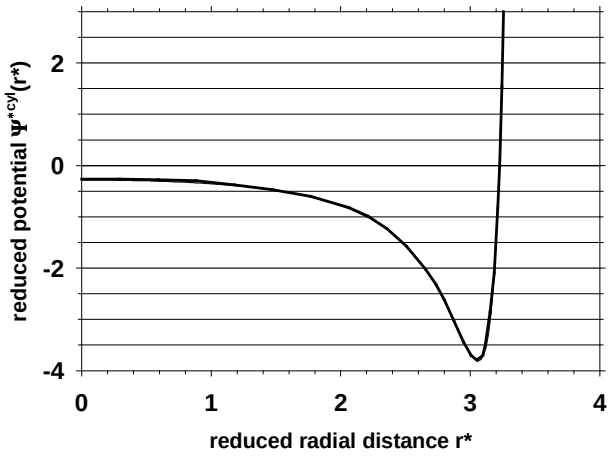
reduced potential Ψ*cyl(r*)
2
0
-2
-4
0
1
2
3
4
reduced radial distance r*

Figure 2

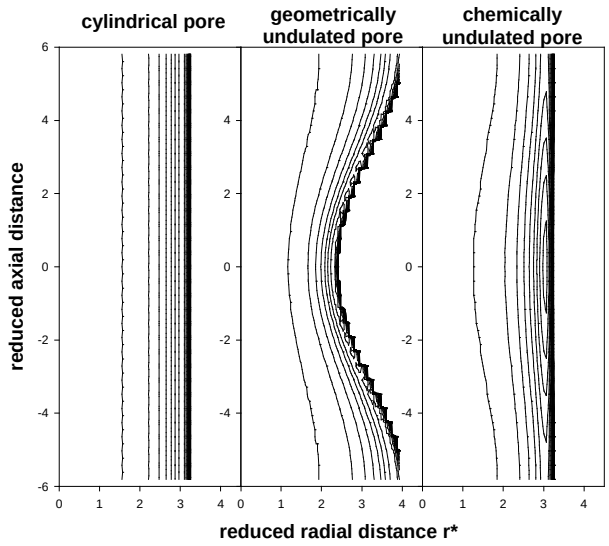
cylindrical pore
geometrically undulated pore
chemically undulated pore
reduced axial distance
reduced radial distance r*
6
4
2
0
-2
-4
-6
0
1
2
3
4

Figure 3

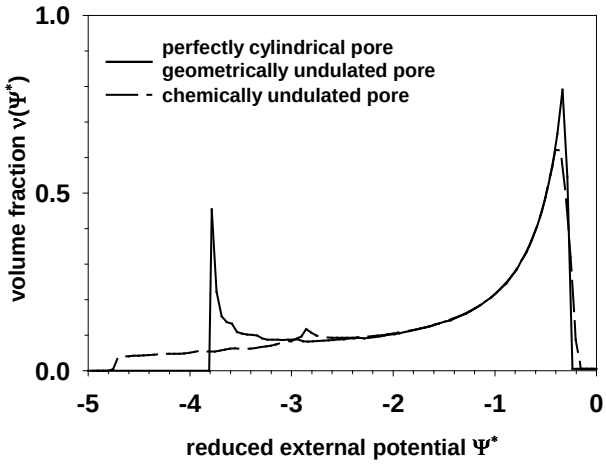
1.0
0.5
0.0
-5
-4
-3
-2
-1
0
volume fraction ν(Ψ*)
reduced external potential Ψ*
perfectly cylindrical pore
geometrically undulated pore
chemically undulated pore

Figure 4

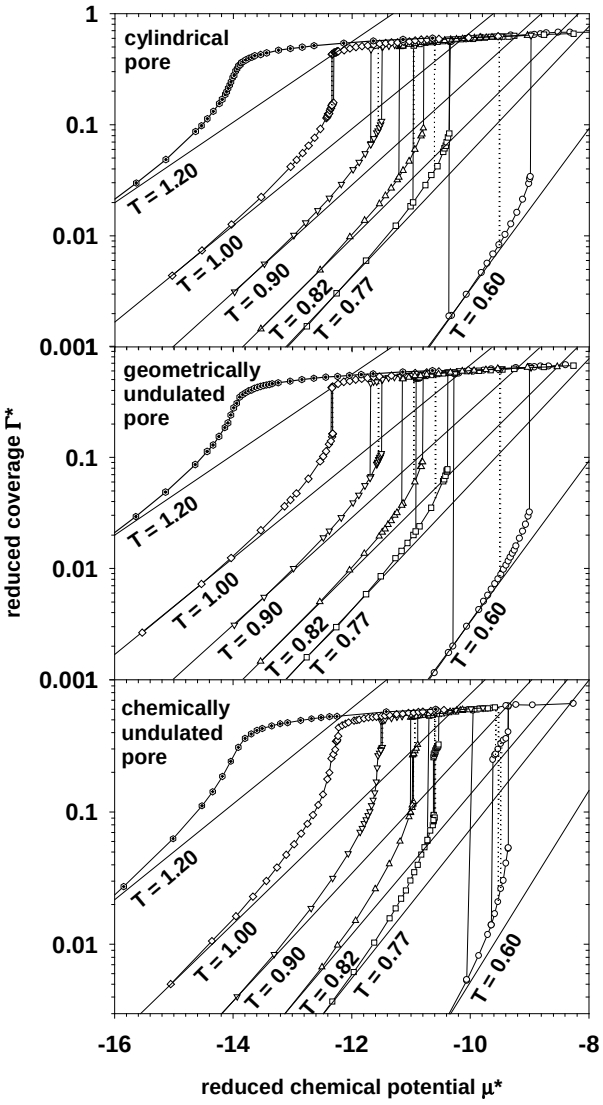
cylindrical pore
geometrically undulated pore
chemically undulated pore
T = 1.20
T = 1.00
T = 0.90
T = 0.82
T = 0.77
T = 0.60
reduced coverage Γ*
reduced chemical potential μ*
1
0.1
0.01
0.001
-16
-14
-12
-10
-8

Figure 5

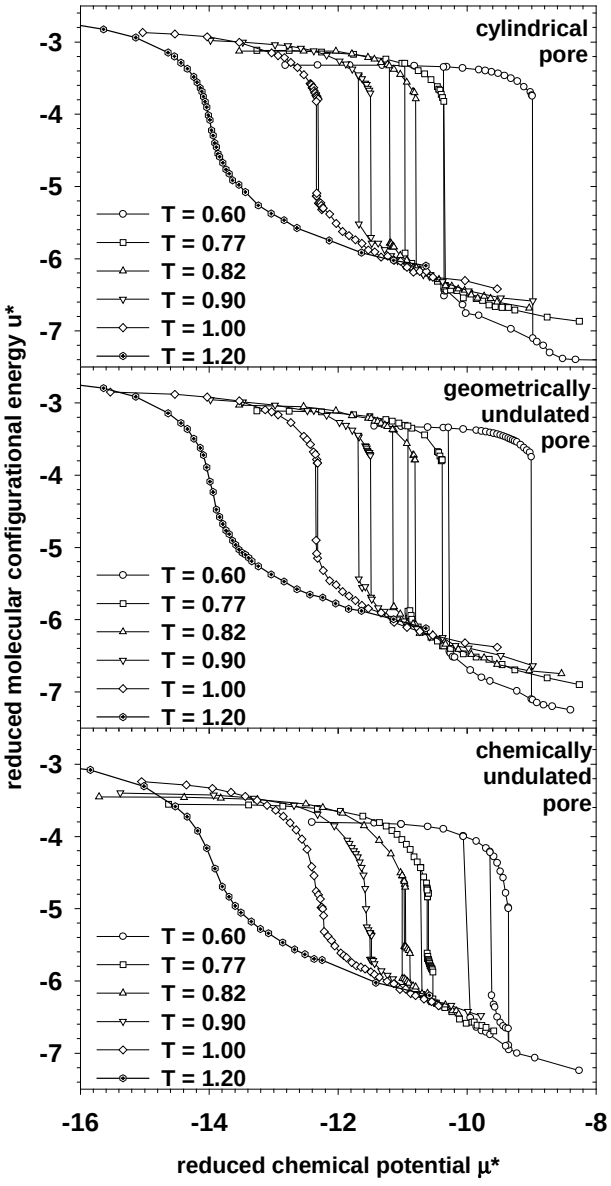
cylindrical pore
geometrically undulated pore
chemically undulated pore
T = 0.60
T = 0.77
T = 0.82
T = 0.90
T = 1.00
T = 1.20
reduced molecular configurational energy u*
reduced chemical potential μ*
-3
-4
-5
-6
-7
-16
-14
-12
-10
-8

Figure 6

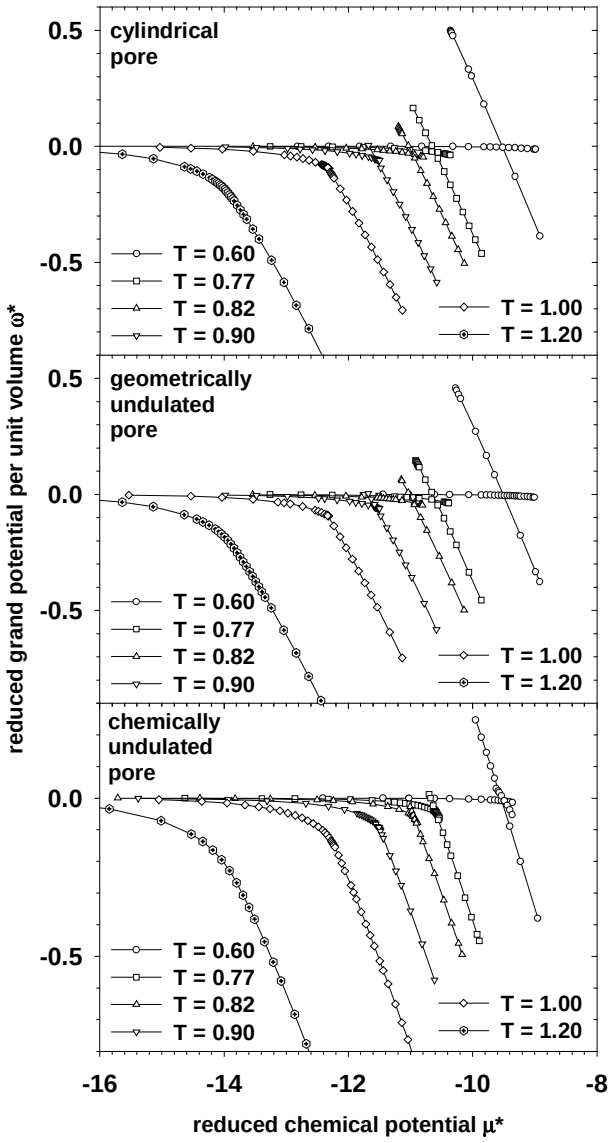
cylindrical pore
geometrically undulated pore
chemically undulated pore
T = 0.60
T = 0.77
T = 0.82
T = 0.90
T = 1.00
T = 1.20
0.5
0.0
-0.5
-16
-14
-12
-10
-8
reduced grand potential per unit volume ω*
reduced chemical potential μ*

Figure 7

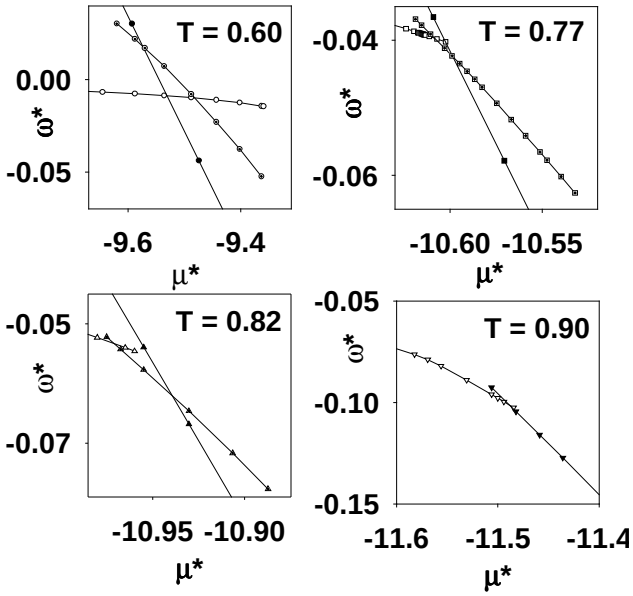
T = 0.60
0.00
-0.05
ω*
-9.6
-9.4
μ*
T = 0.77
-0.04
-0.06
ω*
-10.60
-10.55
μ*
T = 0.82
-0.05
-0.07
ω*
-10.95
-10.90
μ*
T = 0.90
-0.05
-0.10
-0.15
ω*
-11.6
-11.5
-11.4
μ*

Figure 8

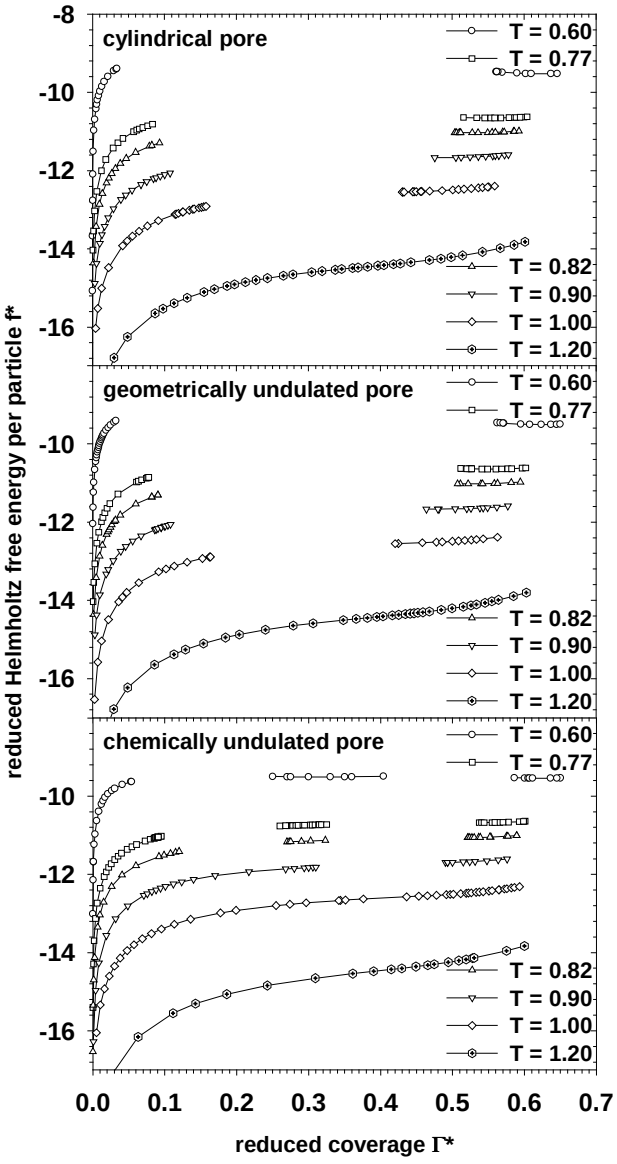
cylindrical pore
geometrically undulated pore
chemically undulated pore
T = 0.60
T = 0.77
T = 0.82
T = 0.90
T = 1.00
T = 1.20
reduced Helmholtz free energy per particle f*
reduced coverage Γ*
-8
-10
-12
-14
-16
0.0
0.1
0.2
0.3
0.4
0.5
0.6
0.7

Figure 9

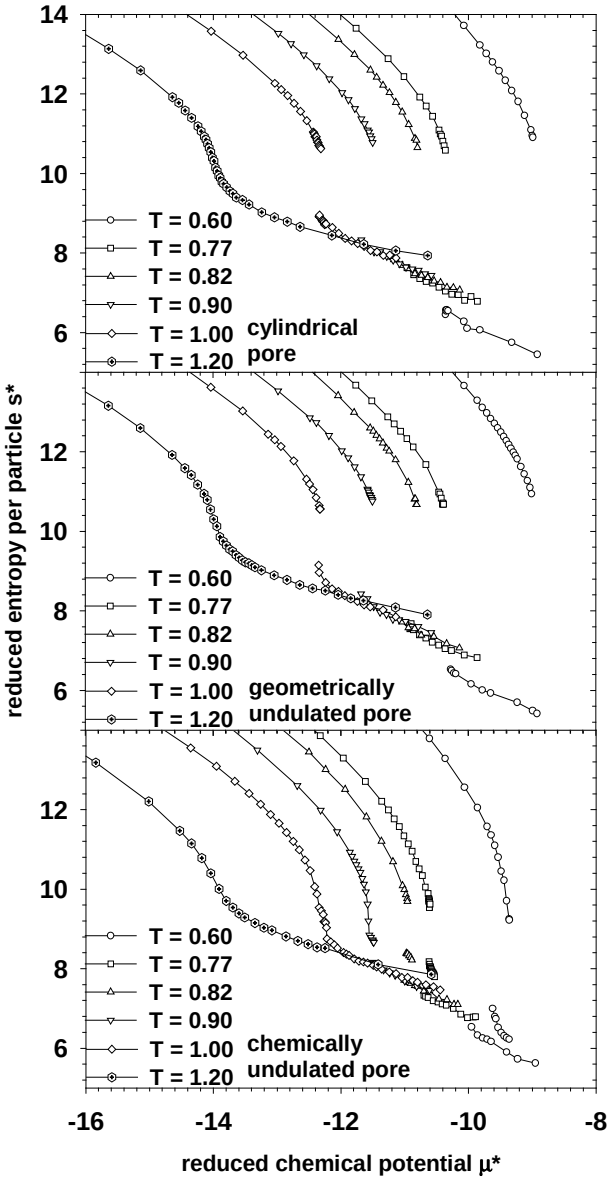
reduced entropy per particle s*
reduced chemical potential μ*
T = 0.60
T = 0.77
T = 0.82
T = 0.90
T = 1.00
T = 1.20
cylindrical pore
geometrically undulated pore
chemically undulated pore